nature communications

Article

https://doi.org/10.1038/s41467-024-53965-0

Development of fin-LEDs for next-generation inorganic displays using face-selective dielectrophoretic assembly

Received: 11 March 2024

Accepted: 28 October 2024

Published online: 04 November 2024

Check for updates

SeungJe Lee[1,5], Yun Jae Eo[1,5], Minji Ko[1], Soomin Ahn[1], Selim Yun[1], Hyeng Jin Kim[1], Eunha Hong[1], Yuna Kwon[1], Huiyeong Kang[1], Yong Jae Lee[1], Gang Yeol Yoo[2], Keyong Nam Lee[1], Jae Kyu Song[3], Jong Kyu Kim[4], Hyun Min Cho[2] & Young Rag Do[1]

Micro-light-emitting diodes offer vibrant colors and energy-efficient performance, holding promise for next-generation inorganic displays. However, their widespread adoption requires the development of cost-effective chips and low-defect pixelation processes. Addressing these challenges, nanorod-light-emitting diodes utilize inkjet and dielectrophoretic assembly techniques. Nevertheless, the small volume and edge-directed emission of nanorod-light-emitting diodes necessitate brightness and light extraction improvements. As an alternative, we propose dielectrophoretic-friendly fin-light-emitting diodes, designed to enhance brightness and light extraction efficiency through face-selective dielectrophoretic assembly technology. Our results confirm the potential for next-generation inorganic displays, with a wafer utilization ratio exceeding 90%, a vertical assembly ratio of 91.3%, and a pixel production yield of 99.93%. Moreover, blue fin-light-emitting diodes achieve an external quantum efficiency of 9.1% and a brightness of 8640 cd m^{-2} at 5.0 V, which, even at this early stage, are comparable to existing technologies.

Micro-light-emitting diodes (Micro-LEDs) have emerged as a key technology in next-generation display technology due to their efficient performance, extended lifespan, wide color gamut, modular capabilities, and stability[1–8]. Notably, several companies have introduced TVs featuring micro-LED technology[9,10]. Apple meanwhile planned to incorporate micro-LED displays in its smartwatch scheduled for release in the future[11,12]. Micro-LEDs are positioned as a possible platform technology for a wide range of applications, from compact screens to giant displays. However, critical challenges remain in micro-LED display production. A significant concern is the need to improve the yield of the pixel manufacturing process while addressing the substantial fabrication costs associated with micro-LED chip production[13–16].

The production cost of micro-LEDs depends on the chip size, assembly speed, and transfer yield. The smaller the chip size is, the faster the assembly speed is, and the higher the transfer yield is, the lower the unit cost is. Supplementary Table 1 provides an overview of chip size, assembly speed, and transfer yield for various micro-LED transfer methods. It is crucial to note that the transfer yield depends on precise positioning of micro-LEDs within pixel grooves. Fluidic self-assembly (FSA) exhibits lower selective transfer rates and requires larger micro-LED chips[10]. In contrast, stamp transfer printing offers the advantages of smaller chip sizes and faster transfer speeds than FSA, albeit with lower repeatability[10]. Despite presenting small chip sizes, rapid transfer speeds, and high accuracy, laser-based transfer is susceptible to LED chip damage when the chip size becomes smaller[17].

[1]Department of Chemistry, Kookmin University, Seoul, Republic of Korea. [2]Display Research Center, Korea Electronics Technology Institute, Gyeonggi-do, Republic of Korea. [3]Department of Chemistry, Kyung Hee University, Seoul 130-701, Korea. [4]Department of Materials Science and Engineering, Pohang University of Science and Technology (POSTECH), Pohang-si, Korea. [5]These authors contributed equally: SeungJe Lee, Yun Jae Eo.
e-mail: yrdo@kookmin.ac.kr

Additionally, it relies on specific laser parameters and bonding methods, with the significant drawback of higher initial costs[7–10]. Conventional FSA, laser transfer, and stamp transfer have respective strengths and weaknesses, but each method has critical issues that must be solved prior to commercializing low-cost micro-LEDs.

One of the micro-LED transfer methods with various sizes, ranging from nano to micrometer, reported to date combines the FSA and dielectrophoretic (DEP) methods. DEP is a method of moving materials by controlling the movement of particles under a non-uniform electric field. This is promising for effectively aligning under 10 micron micro-LEDs as it can quickly move particles to a selective location depending on the strength of the electric field[18]. LG Electronics (LGE) recently expanded the FSA-DEP approach by aligning ~40 μm micro-LEDs into subpixel grooves and assembling them using DEP force within the groove through a positive DEP field and secondary magnetic field to improve the site and face-selectivity of micro-LEDs, which cannot be achieved in conventional FSA with high production yield[19]. In contrast, our team introduced an alternative display device and manufacturing process using nanorod-LEDs to effectively address the high material cost of micro-LEDs and the low assembly speed of conventional FSA processes[20,21]. Following the license and technical assistance of nanorod-LED display technology from our team, the Samsung Display Corporation (SDC) has successfully demonstrated the practical possibility of the DEP process by fabricating a nanorod-LED-based electroluminescent (EL) device through the FSA-DEP process and inkjet printing process[20–26] These reports demonstrate the various advantages of the inkjet-DEP process, such as low-cost nanorod materials, fast assembly speed matched with commercial inkjet speed, and high possibility of transfer yield, promising a viable approach for micro-LED manufacturing[27,28]. However, the horizontal orientation of nanorod-LEDs leads to lateral light emission spread, causing limited multiple quantum well (MQW) volume and diminished forward-directed light emission[20,21], as depicted in Fig. 1a.

This study suggests adopting fin-LEDs to overcome the challenges presented by nanorod-LEDs and the high costs associated with micro-LED displays. Fin-LEDs are similar in size to nanorod-LEDs and are distinguished by the orientation of the p-GaN/MQW/n-GaN structure, aligned parallel to the long axis of fin-LEDs. Featuring a vertical LED device structure, the fin-LED shows a substantial ~eightfold increase in MQW volume compared to nanorod-LEDs, leading to enhanced forward-directed light emission (Fig. 1a). This effect intensifies when fin-LEDs are face-selectively arranged on lower assembly electrodes,

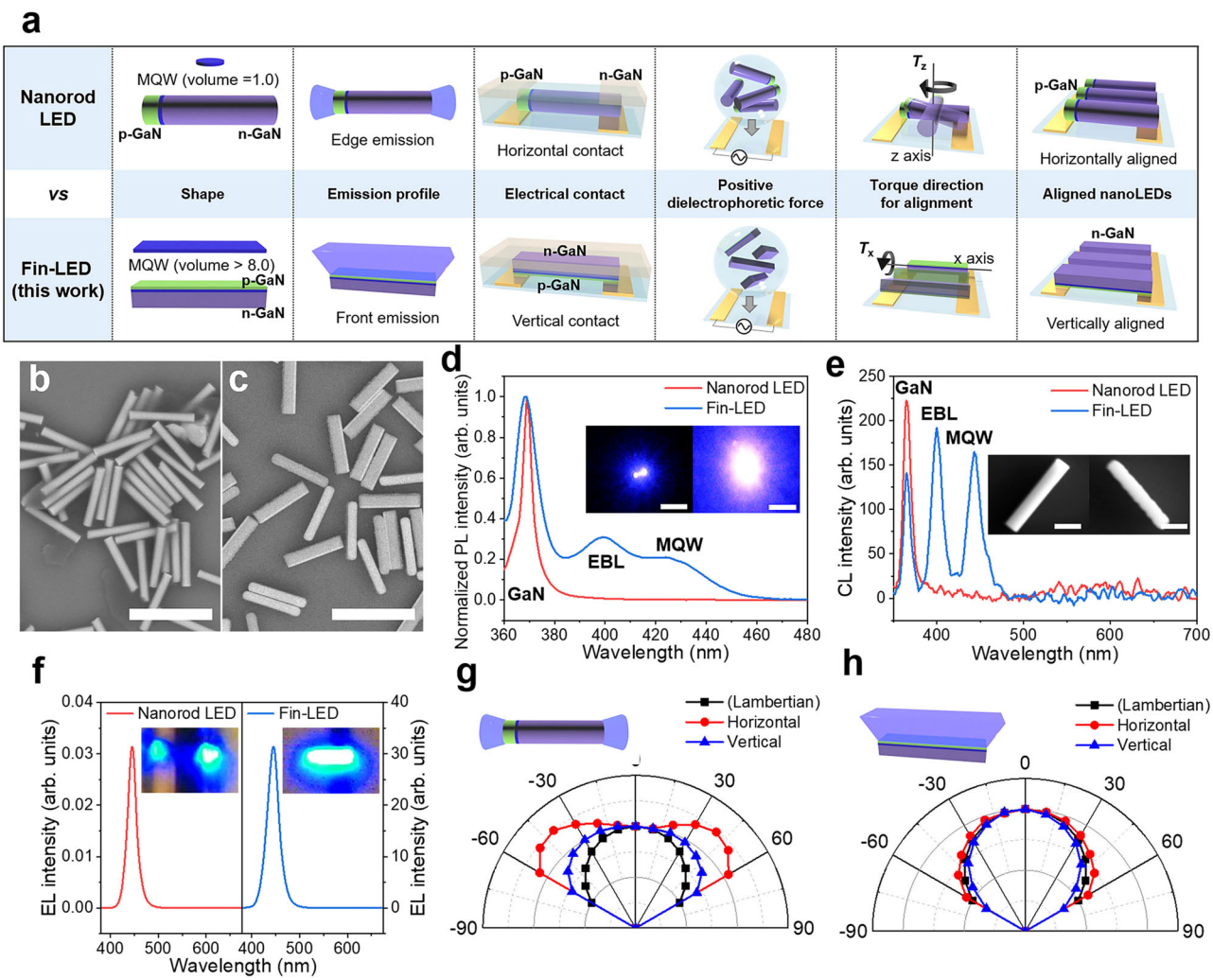

Fig. 1 | Optical characteristics of the fabricated conventional nanorod LED and fin-LED. a Schematic comparison of nanorod LED and fin-LED. Optical characteristics of fabricated conventional nanorod LED and fin-LED. **b** SEM images of individually separated nanorod LED. **c** SEM images of individually separated fin-LED. All scale bars represent 5 μm. **d** PL spectra of nanorod LED and fin-LED under excitation light with a wavelength of 355 nm (Inset: PL emission images of nanorod LED and fin-LED, scale bars represent 10 μm). **e** CL spectra of nanorod LED and fin-LED (Inset image: panchromatic CL images of nanorod LED and fin-LED, scale bars represent 1 μm). **f** EL spectra of nanorod LED and fin-LED under an applied voltage of 8 V. Inset: EL emission images of nanorod LED (left) and fin-LED (right). **g**, **h** Normalized emission angular profiles of single nanorod LED and fin-LED.

concentrating light emission primarily on the front side. The vertical structure of fin-LEDs demands precise alignment for the p-GaN or n-GaN side with the lower assembly electrode to ensure their optical functionality. The DEP field induces motion in fin-LEDs through positive-DEP (p-DEP) movement, attracting them perpendicularly between interdigitated electrodes[18,21,26,29,30]. Achieving the desired face-selective assemblies involves critical rotation around the long axis and optimizing DEP assembly parameters, such as shell and electrode material, solvent type, applied frequency, and voltage, for precise placement on bottom electrodes within subpixels. As indicated in prior reports (Supplementary Table 2), the alignment yield for nanorod-LEDs reached a maximum of 74.4% using DEP assembly[21]. In contrast, our study attains a 91.3% vertical assembly percentage with face-selective DEP, enabling the creation of brighter, vertically structured fin-LED devices and displays. Therefore, the DEP method of nanorod-LEDs is enhanced by a combined approach involving rotation around the short axis by the asymmetric field for horizontal alignment and inkjet printing for site-selective assembly. In the case of larger micro-LEDs, the DEP approach is improved by using chip-shaped grooves for site selectivity and additional magnetic fields for face-selective vertical alignment. Here, the DEP of fin-LEDs is enhanced by rotating around a long axis with specific design adjustments for face-selective vertical alignment without secondary force. This technique appears complex but is successfully demonstrated in this study and remains unreported.

As shown in Supplementary Table 2, much higher brightness can be achieved when fin-LEDs are aligned vertically while having a high assembly percentage, whereas horizontally aligned nanorod-LEDs have either low brightness or are not mentioned. As previously reported, employing DEP assembly techniques featuring double or triple-shelled nanorod-LEDs with dimensions measuring 600 nm in diameter and 4–5 μm in length, they fabricated EL test devices that achieved external quantum efficiency (EQE) levels ranging from 20.2 to 22.2%[27,28]. Previous papers claiming the highest EQE seldom report brightness data. On the other hand, our fin-LED, emitting blue light at a wavelength of 448 nm, achieves a reasonable EQE of 9.1% and a peak luminance of 8640 cd m^{-2} at 5 V. This EQE is comparable to the best EQE of nanorod-LEDs reported without using a high indium-doped wafer, especially at wavelengths below 455 nm[28]. In addition, the brightness of fin-LEDs is much higher than that of other reported nanorod data[18,20,21,27,28].

Fin-LEDs and nanorod-LEDs, due to their similar shapes and sizes, are well-suited for a color-by-blue approach using quantum dots (QDs). The integration of inkjet and DEP techniques allows us to achieve a full-color display with fin-LEDs, as depicted in Supplementary Fig. 1[31–34]. Additionally, we can use inkjet technology to apply a QD-based color conversion layer onto red (R) and green (G) subpixels, achieving a wide-gamut RGB color spectrum. The inkjet-DEP process for fin-LEDs can effectively overcome transfer challenges typically encountered with micro-LEDs, even though the conventional FSA method used in this paper allows the assembly of fin-LEDs with somewhat high assembly speed and transfer yield. Similar to the nanorod-LEDs, the tiny fin-LED can use inkjet printing to improve site selectivity, transfer yield, and speed and reduce material cost[27,35]. This face-selective DEP-based fin-LED assembly process offers notable advantages, including preventing chip damage, achieving rapid assembly speed, and attaining a high pixelation fabrication yield exceeding 99.93%. Our results position this process as a promising technology for creating next-generation inorganic displays.

Results

Fin-light-emitting diodes vs nanorod-light-emitting diodes

We fabricated fin-LEDs in large quantities (tens of millions) from a 4-inch wafer using a top-down etching process, as illustrated in Supplementary Fig. 2. This fabrication process involved nanoimprint lithography, dry etching, and electrochemical etching separation, and thus is highly suitable for mass production. Furthermore, when separating the fin-LEDs from the wafer, the wafer yield remained consistently at 90% or higher[36]. Figure 1b shows an SEM image comparing the fabricated fin-LED and nanorod LED. Fin-LEDs have similar volumes and surface areas as nanorod LEDs but exhibit superior optical properties due to their vertical emission and large MQW area. Vertical emission corresponds to the direction perceived by the eye. Supplementary Fig. 3 displays the results of various measurements, including transmission electron microscope (TEM), X-ray diffraction (XRD), Raman, energy dispersive X-ray spectroscopy (EDS), and secondary ion mass spectrometry (SIMS), which indicate that the crystal structure, composition distribution, and lattice phonon characteristics of the mass-produced fin-LEDs closely match those of typical p-GaN/MQW/n-GaN LEDs.

The critical point is that fin-LEDs have approximately eight times greater InGaN MQW layer volume than nanorod-LEDs, resulting in a significantly enhanced emission volume. Additionally, in the fabrication process of fin-LEDs, the MQW layer is exposed to etching gas and plasma for a shorter time than nanorod-LEDs, leading to a considerably decreased surface-defect density. In Fig. 1c, photoluminescence (PL) images of a single LED under laser excitation highlight the stronger emission of fin-LEDs compared to nanorod-LEDs. In the case of nanorod-LEDs, the smaller MQW volume limits blue light emission, which is concealed within the 368 nm main emission peak of GaN. In contrast, fin-LEDs, with their larger MQW volume, exhibit more robust emissions at both 440 nm and 405 nm, corresponding to MQW and electron-blocking layer (EBL) emissions, as illustrated in Fig. 1d. The enhancement in brightness in fin-LEDs is further confirmed through cathodoluminescence (CL) spectra, demonstrating that the MQW blue emission in fin-LEDs shows a 20-fold increase in emission intensity at 446 nm. Both PL and CL measurements validate that the intense blue peaks observed in single fin-LEDs result from the increased MQW emitting volume and the decreased defect density.

The differences observed in the PL and CL spectra between nanorod-LEDs and fin-LEDs can be attributed to their distinct structural features. In nanorod-LEDs, the relative GaN volume (including p-GaN and n-GaN) is notably larger than that of the MQW and EBL of fin-LEDs. This relative volume difference contributes to the more prominent appearance of the GaN peak in the normalized PL and CL spectra of nanorod-LEDs. Because of their predominantly vertical light emission, vertically oriented fin-LEDs outperform horizontally oriented nanorod-LEDs in outcoupling light from EL devices. Whereas c-plane nanorods, when horizontally aligned, emit light at their ends, with the emitted light directed horizontally toward the MQW layer due to the waveguide effect influenced by the high refractive index of the GaN nanorods, vertically arranged fin-LEDs emit light from the MQW that is predominantly directed toward the front of the EL device. EL images in Fig. 1e visually confirm this phenomenon, showing edge emission for nanorods and front emission for fin-LEDs. Angular-dependent measurements of emitted light illustrate the EL emission profiles of nanorod-LEDs and fin-LEDs, as shown in Fig. 1f, g, in which fin-LEDs exhibit a Lambertian emission pattern.

Simulation of various fin-light-emitting diode structures

The similar shapes of fin-LEDs and nanorod-LEDs allow alignment on two electrodes using DEP assembly. Figure 2a–d compares random and regular fin-LED alignments with and without DEP assembly. Fin-LEDs undergo p-DEP under specific frequencies, aligning between interdigitated electrodes through force and torque. They rotate along the x-axis, reaching positions toward the bottom electrode with the desired orientation. Fin-LEDs align in three face configurations: p-GaN face, shell face, and n-GaN face (Fig. 2e). SEM images (Fig. 2f) illustrate these configurations and misaligned structures. A systematic analysis enabled meticulous evaluation and calculation of vertical alignment ratios for each face configuration.

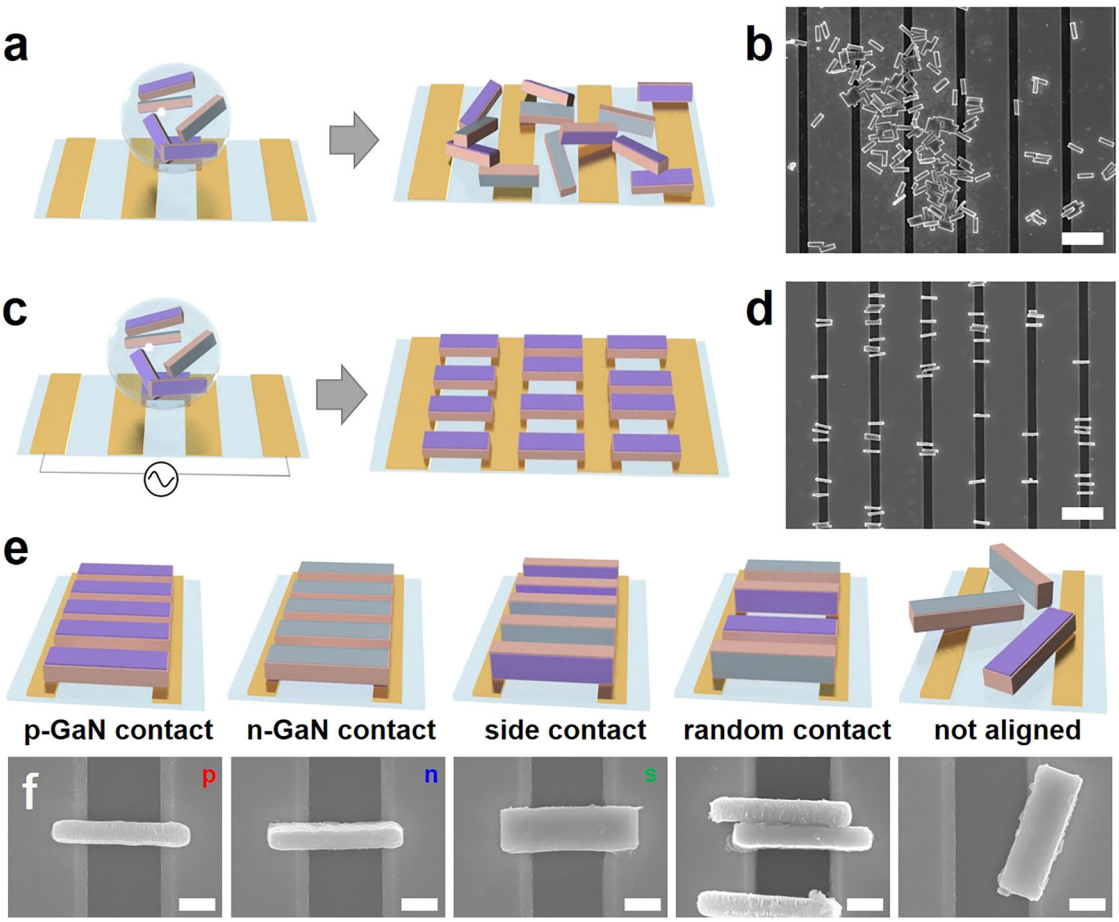

Fig. 2 | Schematic of assembly of individually separated fin-LEDs on pre-patterned electrodes. a, **b** Schematic and SEM results image of fin-LED solution dropped without applying voltage to electrodes. **c**, **d** Schematic and SEM result images of self-assembled fin-LEDs under DEP force. **e**, **f** schematic and SEM result images of fin-LEDs assembled on electrodes in various orientations. Scale bars in (**b**) and (**d**) represent 10 μm and that in (**f**) represents 1 μm.

In preliminary experiments, we noted variations in the alignment of fin-LEDs on the electrode with changes in the DEP factor. To elucidate this phenomenon, we conducted simplified simulations using the Maxwell stress tensor (MST) method and the finite element method (FEM). The dipole approximation method, suitable for simple, spherical particles, introduces substantial errors for elongated particles such as fin-LEDs due to electric field variations along the particles[37]. Therefore, we employed the MST method, which is crucial for evaluating DEP forces and torques, especially for complex structures. Utilizing the near-field approximation, the MST method with the neglected magnetic field can be expressed as follows[38]:

$$\sigma^{\mathrm{MST}} = \tilde{\varepsilon}\left(\mathbf{EE} - \frac{1}{2}(\mathbf{E}\cdot\mathbf{E})\mathbf{I}\right) \tag{1}$$

where $\tilde{\varepsilon}$ is the complex electrical permittivity, **E** is the electric field, and **I** is the unit tensor. The MST is computed using the FEM, a stress analysis technique. In particular, the space around the fin-LED and the surrounding medium is discretized into finite-sized particles, and the MST is integrated over the surface volume of the fin-LED. Therefore, DEP force and torque can be calculated as follows:

$$\mathbf{F}_{\mathrm{DEP}} = \oint_S \langle \sigma^{\mathrm{MST}} \rangle \cdot \mathbf{n} dS \tag{2}$$

$$\mathbf{T}_{\mathrm{DEP}} = \oint_S \mathbf{r} \times \langle \sigma^{\mathrm{MST}} \rangle \cdot \mathbf{n} dS \tag{3}$$

where S represents the surface area of a particle, in this case, the fin-LED, **n** is the normal vector, and **r** is a vector connecting the torque axis to the surface. We used numerical modeling to analyze the DEP force and torque acting on a single fin-LED within the simulation domain, as illustrated in Supplementary Fig. 4. The physical properties of the fin-LED materials, specifically the dielectric constant and electrical conductivity, were taken from Supplementary Table 3 for simulation purposes. To selectively place the p-GaN side of the fin-LED in contact with the electrode, specific conditions must be met for the DEP force and torque. In Fig. 3a, for alignment on the electrodes, the fin-LED dispersed in the solution must experience p-DEP and move toward the side of the stronger electric field, with the negative DEP force in the z-axis direction. When a sinusoidal function with a voltage of 20 V_{pp} and a frequency of 10 kHz is applied to both ends of the metal electrodes, the fin-LEDs with three different structures—fin-LED, ITO/fin-LED, and ITO/fin-LED@SiO_2—all experience p-DEP regardless of the initial rotation angle, as shown in Fig. 3b. Notably, when a SiO_2 shell is present on the LED side, there is a significant force difference depending on the initial rotation angle due to SiO_2 being an electrical insulator. Nevertheless, this type of LED can sufficiently move toward the assembly electrode by p-DEP. Supplementary Fig. 5 shows additional simulation results when the center coordinates of the LED with a SiO_2 shell move in the x- and z-axis directions.

Figure 3c introduces the concept that depending on the initial rotation angle, the DEP torque must be sufficient for selective alignment. In other words, the fin-LED must rotate to position the desired side on the electrode. Suppose the DEP torque acting on the fin-LED is insufficient. In that case, the DEP force may cause the LED to contact

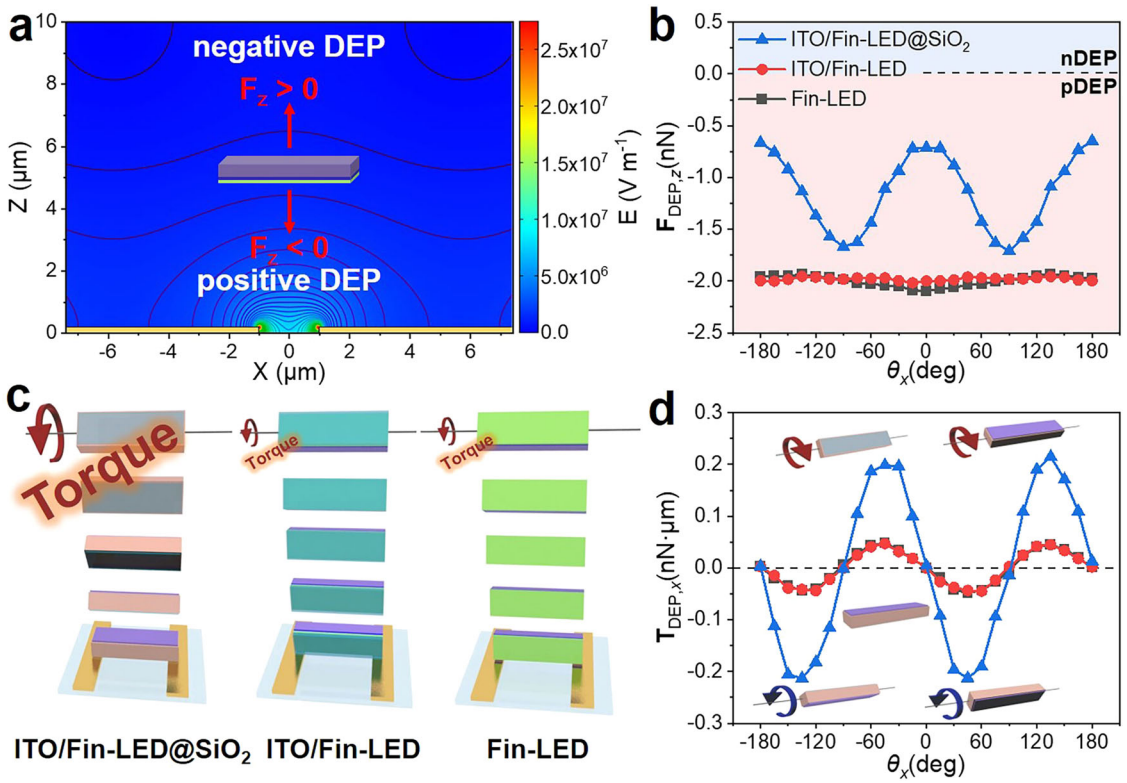

Fig. 3 | FEM simulation results for single fin-LED. a Electric field simulation results. As the color changes from red to blue, the electric field weakens. The isolines are the electric field. **b** *x*-axis DEP force as function of LED structure and *x*-angle when central coordinates of LED were (0 μm, 0 μm, +2 μm) under applied power conditions of 20 V_{pp} and 10 kHz. **c** Torque differences according to fin-LED structure. **d** *x*-axis DEP torque as functions of LED structure and *x*-angle when central coordinates of LED were (0 μm, 0 μm, +2 μm) under applied power conditions of 20 V_{pp} and 10 kHz. The legends of (**b**) and (**d**) are identical; see Supplementary Fig. 4 for simulation details.

the electrode before completing selective alignment, rendering selective alignment impossible. In this regard, the ITO/fin-LED with a SiO_2 shell shows greater torque at the same initial rotation angle than LEDs with other structures, as presented in Fig. 3d. The simulation results exhibit periodic torque variations based on the initial rotation angle; however, these variations cannot fully explain the selective alignment of the fin-LED. Unlike the actual appearance, the simulation assumed a straight cuboid shape for the fin-LED. It did not consider the deformation of the n-GaN layer caused by the electrochemical etching (ECE) method used during the individual separation of fin-LEDs from the wafer. The n-GaN layer with ECE-induced pores may have physical constants that are different from those of conventional n-GaNs, potentially leading to lower electrical conductivity[35]. These differences in physical properties could result in changes in DEP torque depending on the initial rotation angle, and there is experimental evidence to support this observation.

Face-selective assembly of fin-light-emitting diodes

We fabricated a group of fin-LED configurations featuring different fin structures (fin-LED, fin-LED@SiO_2, ITO/fin-LED, and ITO/fin-LED@SiO_2) to compare face-selective assembly (SEM images in Supplementary Fig. 6a–d). We conducted DEP assembly tests on four distinct fin-LED structures, visually represented in Fig. 4a–d. Baseline conditions were established at a frequency of 10 kHz and a voltage of 20 V_{pp}. Various fin-LEDs dispersed in acetone underwent self-assembly on the electrode surface. Self-assembly results for the basic fin-LED structure revealed that a significant number of LEDs were not assembled, and the assembled LEDs were mainly randomly assembled on the side and n-GaN face contacts (Fig. 4a, e). Adding a SiO_2 shell to the side of the fin-LED (fin-LED@SiO_2) reduced the total alignment of the LEDs compared to the assembled result of the basic fin-LED, but increased the fraction of LEDs aligned to the n-GaN face (Fig. 4b, f). These differences occurred because the electrical conductivity of SiO_2 used as the shell material was lower than that of the medium. As simple examples, spherical particles composed of SiO_2 experience negative-DEP (n-DEP) in a similar low-frequency range as used for self-assembly of fin-LEDs, while spherical particles composed of GaN experience p-GaN in that frequency range[39,40]. Therefore, it is intuitively clear that when the fin-LED@SiO_2 with coexisting p- and n-GaN and SiO_2 experiences DEP, the face on which the LED is aligned on the electrodes is determined by the exposed material. Because the magnitude of the electric field increases closer to the electrode, the n-GaN side, which has the highest electrical conductivity among the constituent materials of the fin-LED@SiO_2, tends to face the electrode. For this reason, it is obvious that ITO/fin-LED in which an ITO layer having much higher electrical conductivity than n-GaN is added on p-GaN has a greater proportion of LEDs aligned with the p-GaN side than the n-GaN side on electrodes (Fig. 4c, g). Similar to the basic fin-LED alignment results, the high proportion of ITO/fin-LED aligned on the side is due to the exposure of the side (GaN epi- and ITO layers) of the LED. Ultimately, further substantiating these findings, the SEM image of the ITO/fin-LED@SiO_2 structure revealed that approximately 91.3% of fin-LEDs exhibited selective assembly with a downward orientation, establishing contact between the ITO layer of p-GaN and the bottom electrodes (Fig. 4d). It was also noted that most ITO/fin-LED@SiO_2 displayed alignment tendencies spanning two interdigitated electrodes (Fig. 4h).

We conducted additional assembly experiments based on the ITO/fin-LED@shell structure with various shell materials (ITO/fin-LED@SiO_2, ITO/fin-LED@TiO_2, ITO/fin-LED@SiN_x, and ITO/fin-

LED@SiO_2/Al_2O_3/SiO_2) under identical conditions (Supplementary Fig. 6d–g). Face-selective assembly was only possible using low dielectric constant SiN_x, SiO_2, and triple-shelling ITO/fin-LEDs. In contrast, the high dielectric constant shell of the ITO/fin-LED@TiO_2 structure did not lead to face-selective alignment, as shown in Supplementary Fig. 7. These results suggest that face-selective assembly is achievable when the dielectric constant of the shelling material surrounding the fin-LED is lower than that of the medium.

We also compared alignment based on the ITO/fin-LED@SiO_2 structure as a function of the solvent and determined the optimal face-selective alignment. We performed experiments by comparing their dielectric constants for each medium (hexane, acetone, and IPA). Supplementary Fig. 8a illustrates the results of face-selective alignment as a function of applied voltage when the medium is hexane. In addition to the lack of p- or n-GaN face-selective alignment, many fin-LEDs remained unaligned between the electrodes. However, Supplementary Fig. 8b, c demonstrates that acetone and IPA enable face-selective alignment of over 90% between 20 to 40 V_{pp} as the dielectric constant of the medium increases. These results indicate that face-selective alignment is more achievable when the dielectric constant of the medium is higher, that is, when the difference in the dielectric constant between the medium and the shell material of the fin-LED is larger. Supplementary Fig. 8d confirms that face-selective alignment achieves the highest values at applied frequencies between 10^1 and 10^2 kHz under an acetone medium with a voltage of 20 V_{pp}. The decrease in fin-LED rotation at a high frequency of 10^3 kHz can be attributed to the relatively lower x-axis $\mathbf{T}_{DEP}$ values of the fin-LED.

Supplementary Movie 1 demonstrates the rapid and precise alignment of optimized ITO/fin-LED@SiO_2 under an electric field, moving precisely toward the positions of the pixels. LEDs that do not align correctly with the pixels remain in the solvent during assembly. After completion, any misaligned fin-LEDs can be recovered, leaving no LEDs outside the designated pixel areas. Figure 5a, b shows images of bad and good pixels. We defined a bad cell as a pixel with 15 or less but 60 or more fin-LEDs aligned in an area of 42×42 μm^2. This is because fin-LEDs with less than 15 fin-LEDs produce uniform light intensity within the pixel, and fin-LEDs with over 60 fin-LEDs will act as dead pixels due to overlapped alignment of the fin-LEDs. This

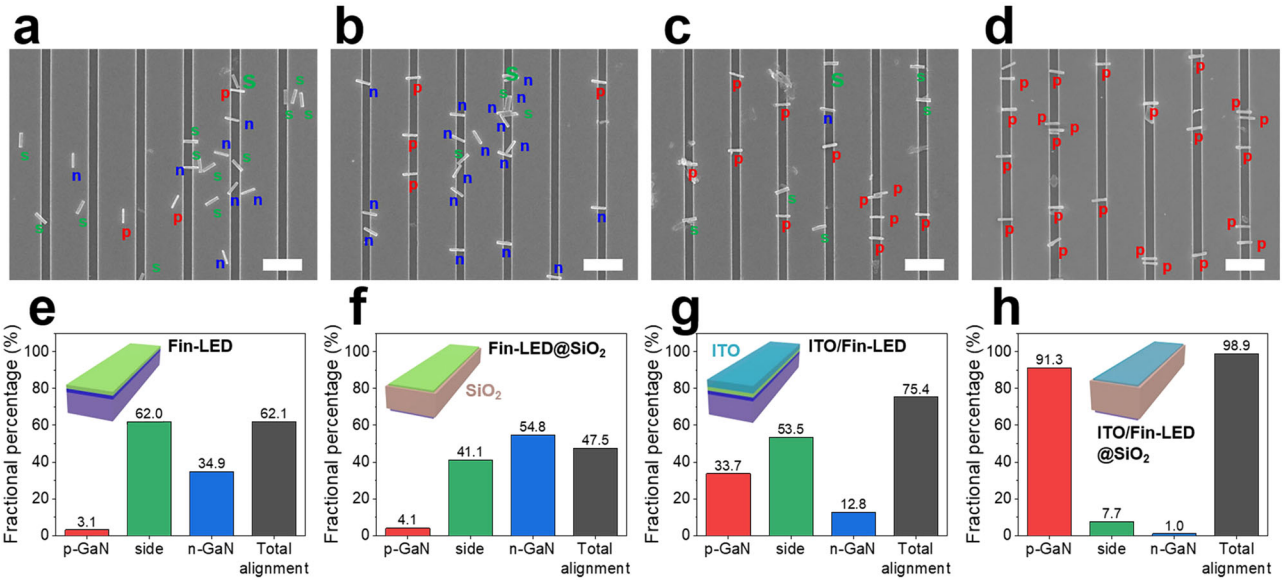

Fig. 4 | Self-assembly results of differently structured fin-LEDs by DEP force. **a**–**d** SEM image of fin-LED, fin-LED@SiO_2, ITO/fin-LED, and ITO/fin-LED@SiO_2 structures. To align the fin-LEDs of all structures, a sinusoidal function with a voltage of 20 V_{pp} and a frequency of 10 kHz was applied to the electrodes. To indicate the contact surface between the fin-LEDs and electrodes, different colored letters were marked on the individual LEDs: red p, p-GaN contact; blue n, n-GaN contact; green s, side contact. **e**–**h** Fractional ratios of different contacts of fin-LED, fin-LED@SiO_2, ITO/fin-LED, and ITO/fin-LED@SiO_2 structures (Scale bar represents 10 μm).

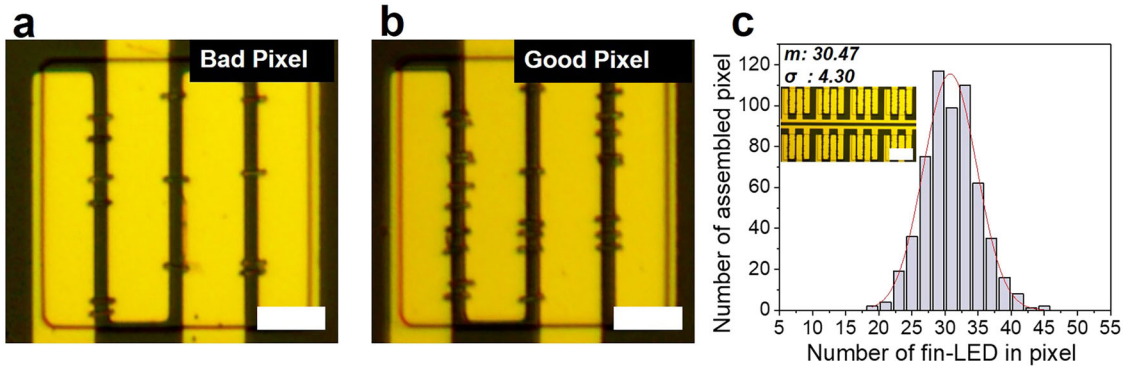

Fig. 5 | DEP alignment of fin-LEDs in the pixel. **a**–**b** Optical microscope (OM) image of Fin-LED Array Cell assembled using DEP method **a** Bad pixel: fin-LED assembled in pixel (number of fin-LEDs: 14 ea) **b** Good pixel: fin-LED assembled in pixel (number of fin-LEDs: 25 ea), Scale bars represent 10 μm. **c** Distribution of fin-LED count per pixel, Inset image: Fin-LED pixel array image (pixel size: 42×42 μm^2). Scale bars represent 40 μm. m mean, σ standard deviation.

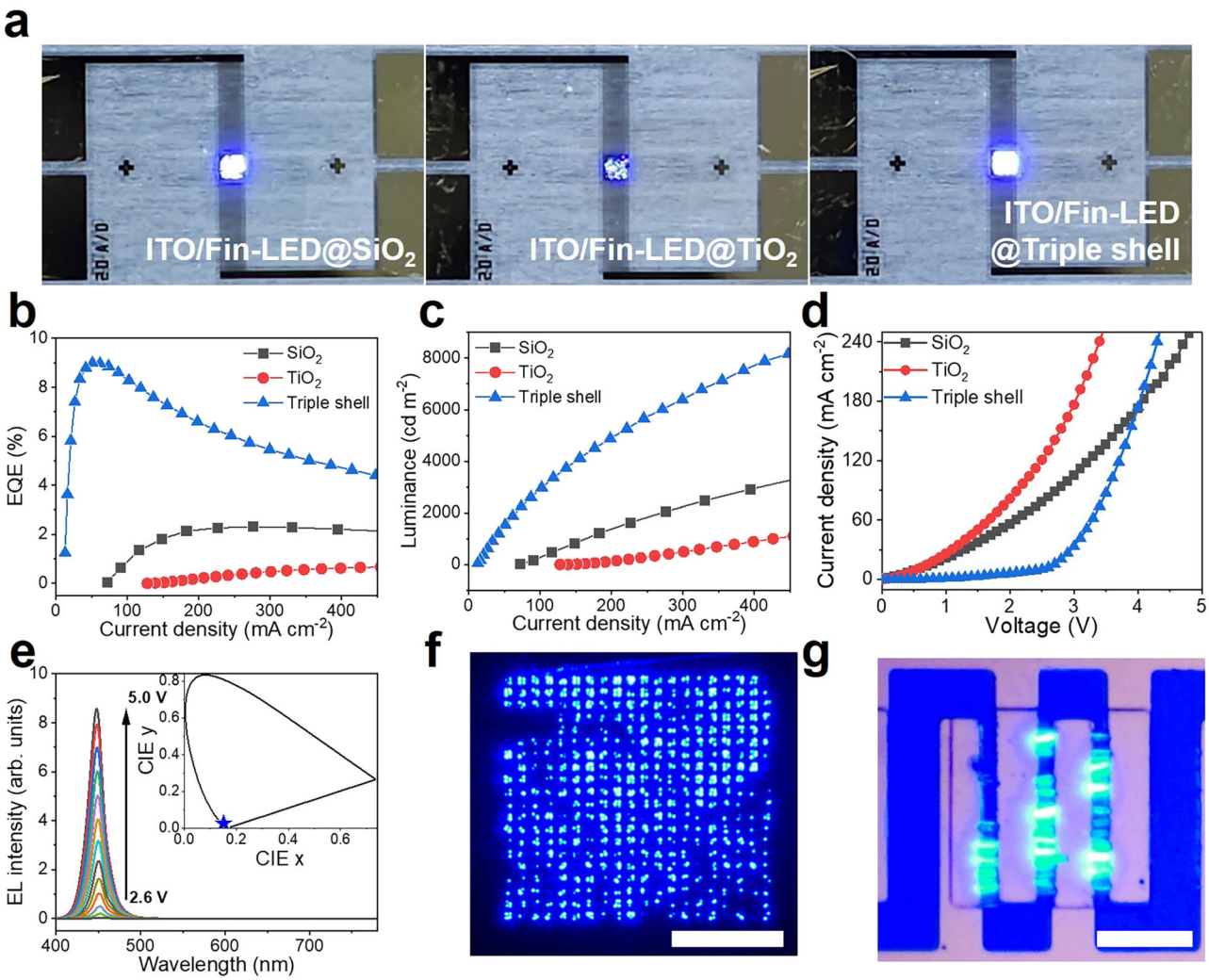

Fig. 6 | EL characteristics of fin-LED devices according to fin-LED shell materials. a Photographs of EL emission images. A voltage of 3.5 V was applied to all devices, and the light emitting area was 1 × 1 mm^2. **b** EQE-current density curve. **c** Luminance-current density (L-J) curve. **d** Current-voltage (I-V) curve in 0 to +5 V range. **e** EL spectra and CIE color coordinates according to current density. **f** Fin-LED array cell emission images of fin-LED array. Scale bar represents 500 μm **g** OM image of fin-LED pixel (fin-LED array: 21 × 28 array / total 588 pixels, pixel size: 42 × 42 μm^2) Scale bar represents 20 μm.

overlapped alignment can cause leakage current during device processing. The fin-LEDs produced five cells with a total of 588 pixels, and only two defective subpixels are found out of a total of 2940 pixels. Based on this assessment, the assembly accuracy reached 99.93%. Furthermore, the aligned fin-LEDs also show a ~91% face-selective alignment ratio, primarily with the p-GaN side facing over the bottom electrode. Supplementary Fig. 9 illustrates the numbers of assembled fin-LEDs on each pixel using DEP and ink-dropping processes within an array cell of 588 subpixels. On average, approximately 30.7 fin-LEDs are assembled on the designated electrodes and aligned within each subpixel, with a standard deviation of 4.07 (Fig. 5c).

Fin-light-emitting diode electroluminescent devices

We fabricated three fin-LED EL devices using TiO_2, SiO_2, and a triple-shell $SiO_2/Al_2O_3/SiO_2$ configuration. These differently aligned EL devices were manufactured using fin-LEDs, employing $SiO_2/Al_2O_3/SiO_2$ triple-shells to reduce surface defects and maintain a high face-selective ratio. Additionally, Al_2O_3 also serves as an etch block layer during device fabrication, and the passivation further complements the E-beam deposition passivation, providing more effective overall passivation[26,27]. Figure 6a visually compares emission images captured from the three types of fin-LED EL devices operated at 5 V. Figure 6a, b confirms that the triple-shell fin-LED EL device outperforms its counterparts, namely the SiO_2-shell and TiO_2-shell, in terms of brightness and uniformity of light emission. The difference between the SiO_2-shell and the TiO_2-shell appears to be due to face-selective alignment. In addition, since the triple shell shows alignment similar to that of the SiO_2 shell, the difference can be attributed to the passivation effect as well as the superiority of surface-selective alignment. Similarly, due to the face-selective effect, the SiO_2-shelled fin-LED demonstrates enhanced efficiency and brightness compared to the TiO_2-shelled variant. Consequently, the triple-shelled fin-LED EL device attains a peak external EQE of 9.1% at a current density of 49.7 mA cm^{-2}. It also exhibits notable luminance, achieving a value of 8640 cd m^{-2} at an applied voltage of 5.0 V. This luminance level surpasses that of the TiO_2-shelled fin-LED EL device by a factor of 10.4 and exceeds that of the SiO_2-shelled counterpart by a factor of 3.2, as shown in Fig. 6b, c. Furthermore, this result is comparable to the best EQE of nanorod-LEDs reported without a high indium-doped wafer, especially at wavelengths below 455 nm. Figure 6d shows the current density-voltage (J-V) curve of the fin-LEDs. The turn-on voltages for SiO_2, TiO_2, and triple-shelled fin-LEDs are 2.6 V, 2.7 V, and 2.6 V, respectively, with brightness at the turn-on voltage of 10.78 cd m^{-2}, 5.1171 cd m^{-2}, and 47.495 cd m^{-2}, respectively. Among these, the triple-shelled fin-LED exhibits the lowest leakage current density. This substantial reduction in leakage current is thus achieved through improved passivation and

face-selective alignment. Figure 6e shows that, compared to micro-LEDs, the fin-LED displays a relatively modest blue shift with increasing applied voltage. This behavior is attributed to the smaller dimensions of fin-LEDs, which mitigate the MQW polarization effect.

Discussion

We successfully developed submicron-scale fin-LEDs, a possible LED structure allowing face-selective assembly. While sharing a size comparable to those of previously developed nanorod-LEDs, our fin-LEDs exhibit Lambertian front emission characteristics, as demonstrated by PL, CL, and EL measurements. Our investigation into the face-selective assembly of three different structures, utilizing simulations including MST and FEM under an electric field, revealed a consistent p-DEP tendency in the fin-LEDs. The ITO/fin-LED@SiO_2 structure exhibited a large DEP torque at the initial rotation angle and displayed periodic torque variations.

Simulations and experiments show that upon DEP alignment, 91.3% of the fin-LEDs in the ITO/fin-LED@SiO_2 structure were in contact with the ITO layer of p-GaN and the bottom electrode. We also confirmed how the alignment is affected by both the dielectric constants and conductivities of the passivation layer and the medium. We fabricate fin-LED EL devices for three-fin-LED structures based on this face-selective alignment ability. The ITO/fin-LED@SiO_2 structure exhibited higher levels of efficiency and brightness than those of the ITO/fin-LED@TiO_2 structure. In particular, the ITO/fin-LED@Triple-shell structure featured face-selective alignment and improved passivation, achieving a maximum EQE of 9.1% and a high luminance of 8640 cd m^{-2} at 5.0 V.

Although at this early stage of fin-LED development, the EQE is slightly lower than those of previously reported nanorod-LEDs, fin-LEDs nonetheless can address the inherent issues facing nanorod-LED and micro-LED technology. Finally, we successfully arranged fin-LEDs in a pixel array and, by doing so, successfully fabricated an array cell for them. We also achieve a pixel production yield of 99.93% through the face-selective assembly of DEP-friendly fin-LEDs. Fin-LEDs inherently exhibit promising optical characteristics, thus further confirming their potential as a next-generation inorganic display technology.

Methods

Fabrication of fin-light-emitting diodes

The experiment utilized a blue epitaxial growth wafer purchased from SEMITEK Co., consisting of a 50 nm p-GaN layer, 150 nm InGaN/GaN MQWs, and a 2.0 μm n-GaN layer. Subsequently, a 150 nm Indium-Tin-Oxide (ITO) layer was deposited using RF-sputtering to serve as the current spreading layer. Following the ITO deposition, we applied a stack of aluminum (Al) and silicon dioxide (SiO_2) layers as a hard etching mask for the GaN material. These layers were deposited with 200 nm and 900 nm thicknesses, respectively. The deposition process utilized a combination of plasma-enhanced chemical vapor deposition (PECVD) and electron beam evaporator technology. We used the nanoimprint lithography method to fabricate fin-LED arrays. To proceed with the nanoimprinting, we spin-coated a layer of spin-on-glass (SOG) material (FOX-16, DOW Corning Co.) onto the polydimethylsiloxane (PDMS, Sylgard® 184, Dow Corning Co.) mold. The SOG-coated PDMS mold was then placed onto the etching-mask-deposited GaN wafer, and pressure was uniformly applied to enable the nanoimprinting process. This process transferred the fin-LED-shaped pattern onto the Al layer at the top of the GaN wafer. The hard mask was made of etched Al and SiO_2 using chlorine-based inductively coupled plasma (ICP) and fluorine-based reactive ion etcher (RIE), respectively. After carving the hard mask, the GaN layer was etched with Cl-based ICP Etch. To reduce the dry etching defect, tetramethylammonium hydroxide (TMAH, 25 wt% in H_2O, Sigma-Aldrich) was applied to the GaN layer at 80 °C for 5 min. To control the excessive formation of pores in the n-GaN layer during the ECE process, 50 nm of SiO_2 was deposited through 50 nm PECVD. Afterward, the bottom part of n-GaN was etched, and ECE was performed in 0.3 M oxalic acid for 5 min to create pores so that the fin-LED could be separated from the wafer. Afterward, the ECE protection layer was removed using a buffer-oxide etchant (BOE), and a passivation layer was deposited. Sonication was performed for 5 min in γ-butyrolactone (GBL) solution to separate the fin-LEDs from the wafer. Finally, the material was purified and replaced with an acetone solution.

Simulation of fin-light-emitting diodes

We used Comsol for fin-LED simulations. The dimensions of the fin-LED were 3.8 μm length, 0.6 μm width, and 0.8 μm height. In these simulations, we set the reference voltage and frequency as sinusoidal functions, with a voltage of 20 V_{pp} and a frequency of 10 kHz. We calculated force and torque based on the dielectric constant and conductivity of the passivation material and the medium. Additionally, we analyzed the variations in force and torque with changes in voltage and frequency.

In our research, we conducted simulations using the MST method, which is particularly suitable for evaluating DEP forces and torques in complex structures such as fin-LEDs. While expressing simulation results through mathematical equations may have limitations, we want to emphasize the critical role of the MST method in our approach. The MST method, relying on complex electrical permittivity ($\tilde{\varepsilon}$), allows us to calculate DEP forces and torques accurately. By integrating the MST over the surface volume of the fin-LED within a FEM analysis, we can derive the DEP force ($\mathbf{F}_{DEP}$) and DEP torque ($\mathbf{T}_{DEP}$). These calculations consider factors such as surface area (S), the normal vector ($\mathbf{n}$), and the vector connecting the torque axis to the surface ($\mathbf{r}$). While expressing the simulation results mathematically beyond these equations may be challenging, it is important to note that our simulations focused on accuracy and numerical modeling. We acknowledge that modeling the exact shape of fin-LEDs and considering real-world factors, such as the deformation of the n-GaN layer caused by the ECE method during the individual separation of fin-LEDs from the wafer, can be complex.

Fabrication of electroluminescent devices

A function generator (Handyscope HS5; TiePie Engineering, Netherlands) and a voltage amplifier (A400; FLC Electronics, Sweden) were used to align the individually separated fin-LEDs on the interdigitated electrodes. Fin-LEDs were assembled by dropping separated fin-LEDs from an ink solution into acetone while applying a sinusoidal function with a voltage of 20 V_{pp} and a frequency of 10 kHz to both ends of the metal electrodes. Subsequently, an insulating layer of SiO_2 and SU-8 was applied to cover the interdigitated electrode area where the fin-LEDs were aligned. Oxygen and fluorine-based RIE were performed to establish the contact between the fin-LED and the top electrode. Finally, a transparent electrode with a thickness of 500 nm made of aluminum-doped zinc oxide (AZO) was deposited.

Characterization

The manufacturing process of fin-LEDs was confirmed using scanning electron microscopy (SEM; JSM-7610F, JEOL Ltd., Japan). The fin-LEDs array substrate was characterized by X-ray diffraction (XRD; Ultima IV, Rigaku), Raman microscopy (Nd:YAG laser, λ = 532 nm), and secondary ion mass spectrometry (SIMS; IMS 6F, CAMECA, France). The material properties of individually separated fin-LEDs were characterized by transmission electron microscopy (TEM; JEM-2100F, JEOL Ltd., Japan) with an acceleration voltage of 200 kV.

Cathodoluminescence measurements

Ink dispersed in acetone is prepared and dropped onto a silicon substrate using a micropipette for nanorod LEDs and fin-LEDs. Subsequently, the residual solvent is removed on a hot plate at 150 °C. CL characteristics are then examined using a SEM-CL (MONO CL3+, Gatan,

Inc., USA) with an electron beam accelerated to 15 kV at room temperature. The measurements are conducted at a magnification of 20×, and the measured spectrum covers a range of 300 to 800 nm.

Micro-photoluminescence measurements

Nanorod LEDs and fin-LEDs are prepared by dispersing ink in acetone, followed by dropping this onto a silicon substrate using a micropipette. The residual solvent is completely removed on a hot plate at 150 °C. Subsequently, a single nanorod LED and fin-LED are measured using a He-Cd laser in confocal mode. The laser spot size is 30 μm, and the measurement is carried out with only one LED within a 30 laser spot radius, ensuring no other LEDs are present. In the case of fin-LEDs, p-GaN n-GaN LEDs are measured to align their emission characteristics with the EL.

Electroluminescence and optical microscopy measurements

The electroluminescence spectra and current-voltage-luminance (IVL) characteristics of the fabricated fin-LED EL device were analyzed using a CS-2000 (Konica Minolta, Japan) coupled with a DC power supply (Keithley 2001, Keithley Instruments Inc., USA) as voltage and current sources. A single-emitting nanorod LED and fin-LED are located within the fabricated EL device and measured under 150× magnification.

Data availability

The data that support the plots within this paper and other findings of this study are available from the corresponding author upon request.

References

1. Pust, P., Schmidt, P. J. & Schnick, W. A revolution in lighting. *Nat. Mater.* **14**, 454–458 (2015).
2. Wu, T. et al. Mini-LED and micro-LED: promising candidates for the next generation display technology. *Appl. Sci.* **8**, 1557 (2018).
3. Wierer, J. J. & Tansu, N. III-Nitride micro-LEDs for efficient emissive displays. *Laser Photonics Rev.* **13**, 1900141 (2019).
4. Huang, Y., Hsiang, E.-L., Deng, M.-Y. & Wu, S.-T. Mini-LED, Micro-LED and OLED displays: present status and future perspectives. *Light Sci. Appl.* **9**, 105 (2020).
5. Liu, Y. et al. 53.3: The size and temperature effect of ideality factor in GaN/InGaN multiple quantum wells micro light emitting diodes (micro-LEDs). *SID Symp. Dig. Tech. Pap.* **52**, 387–390 (2021).
6. Do, Y. R. & Yoo, G. Y. MicroLEDs get in line. *Nat. Electron.* **6**, 182–183 (2023).
7. Lee, T.-Y. et al. Technology and applications of micro-LEDs: their characteristics, fabrication, advancement, and challenges. *ACS Photonics* **9**, 2905–2930 (2022).
8. Miao, W. et al. Microdisplays: mini-LED, micro-OLED, and micro-LED. *Adv. Opt. Mater.* **12**, 2300112 (2023).
9. Virey, E. H. & Baron, N. 45-1: Status and prospects of microLED Displays. *SID Symp. Dig. Tech. Pap.* **49**, 593–596 (2018).
10. Anwar, A.-R. et al. Recent progress in micro-LED-based display technologies. *Laser Photonics Rev.* **16**, 2100427 (2022).
11. Rossignol, J. Apple watch with micro-LED display and lower-priced AirPods rumored for 2024. *MacRumors* https://www.macrumors.com/2023/01/02/cheaper-airpods-and-micro-led-apple-watch-rumors/ (2023).
12. Charlton, H. Custom microLED displays could be heading to the iPhone, Vision Pro, and Apple Car. *MacRumors* https://www.macrumors.com/2023/08/10/microled-displays-for-iphone-vision-pro-apple-car/ (2023).
13. Liu, Z. et al. Micro-light-emitting diodes with quantum dots in display technology. *Light Sci. Appl.* **9**, 83 (2020).
14. Lee, H. E. et al. Micro light-emitting diodes for display and flexible biomedical applications. *Adv. Funct. Mater.* **29**, 1808075 (2019).
15. Zhang, H. & Rogers, J. A. Recent advances in flexible inorganic light emitting diodes: from materials design to integrated optoelectronic platforms. *Adv. Opt. Mater.* **7**, 1800936 (2019).
16. Chen, D., Chen, Y.-C., Zeng, G., Zhang, D. W. & Lu, H.-L. Integration technology of micro-LED for next-generation display. *Research* **6**, 0047 (2023).
17. Gong, Z. & Gong, Y. Laser-based micro/nano-processing techniques for microscale LEDs and full-color displays. *Adv. Mater. Technol.* **8**, 22200949 (2023).
18. Chang, W. et al. Concurrent self-assembly of RGB microLEDs for next-generation displays. *Nature* **617**, 287–291 (2023).
19. Park, H. K. et al. Horizontally assembled green InGaN nanorod LEDs: scalable polarized surface emitting LEDs using electric-field assisted assembly. *Sci. Rep.* **6**, 28312 (2016).
20. Eo, Y. J. et al. Enhanced DC-operated electroluminescence of forwardly aligned p/MQW/n InGaN nanorod LEDs via DC offset-AC dielectrophoresis. *ACS Appl. Mater. Interfaces* **9**, 37912–37920 (2017).
21. Do, Y. R. Display including nanoscale LED module. US patent US20210151424A1 (2020).
22. Do, Y. R. Nano-scale light-emitting diode (L. E. D.) electrode assembly emitting polarized light, method of manufacturing the same, and polarized LED lamp having the same. US patent US011635176B2 (2020).
23. Do, Y. R. Display including nanoscale LED module. US patent US011538799B2 (2022).
24. Do, Y. R. Display comprising ultra-small LEDs and method for manufacturing same. US patent US009570425B2 (2020).
25. Ryu, J. et al. Technological breakthroughs in chip fabrication, transfer, and color conversion for high-performance micro-LED displays. *Adv. Mater.* **35**, 2204947 (2023).
26. Sheen, M. et al. Highly efficient blue InGaN nanoscale light-emitting diodes. *Nature* **608**, 56–61 (2022).
27. Cho, H., Kim, D., Lee, S., Yoo, C. & Sim, Y. Efficiency enhancement of submicron-size light-emitting diodes by triple dielectric layers. *J. Soc. Inf. Disp.* **31**, 289–297 (2023).
28. Kim, S. et al. Self-array of one-dimensional GaN nanorods using the electric field on dielectrophoresis for the photonic emitters of display pixel. *Nanoscale Adv.* **5**, 1079–1085 (2023).
29. Naieni, A. K. & Nojeh, A. Effect of solution conductivity and electrode shape on the deposition of carbon nanotubes from solution using dielectrophoresis. *Nanotechnology* **23**, 495606 (2012).
30. Freer, E. M., Grachev, O., Duan, X., Martin, S. & Stumbo, D. P. High-yield self-limiting single-nanowire assembly with dielectrophoresis. *Nat. Nanotechnol.* **5**, 525–530 (2010).
31. Do, Y. R. Display device and method for manufacturing display device. US patent US20220102604A1 (2022).
32. Do, Y. R. Display device and manufacturing method therefor. US patent US220220068876A1 (2021).
33. Do, Y. R. Light-emitting device, display device comprising same, and method for manufacturing display device. EPC patent EP 3 913 696 A1 (2021).
34. Do, Y. R. Light-emitting device and display device comprising same. EPC patent EP 3 913 678 A1 (2021).
35. Yun, J. S. & Kim, M. S. Ink composition for electrophoretic device and display device using the same. Korean patent KR 1020210133044A (2021).
36. Ko, M. et al. Development and isolation of dot LEDs for display applications through electrochemical etching and sonochemical separation. *Adv. Funct. Mater.* **34**, 2303727 (2023).
37. Wang, X., Wang, X.-B. & Gascoyne, P. R. C. General expressions for dielectrophoretic force and electrorotational torque derived using the Maxwell stress tensor method. *J. Electrost.* **39**, 277–295 (1997).

38. Green, N. G. & Jones, T. B. Numerical determination of the effective moments of non-spherical particles. *J. Phys. Appl. Phys.* **40**, 78–85 (2007).
39. Morgan, H., Sun, T., Holmes, D., Gawad, S. & Green, N. G. Single cell dielectric spectroscopy. *J. Phys. D Appl. Phys.* **40**, 61–70 (2007).
40. Kumar, S. & Hesketh, P. J. Interpretation of ac dielectrophoretic behavior of tin oxide nanobelts using Maxwell stress tensor approach modeling. *Sens. Actuators B Chem.* **161**, 1198–1208 (2012).

Acknowledgements

This work was supported by the Ministry of Trade, Industry and Energy (MOTIE), Republic of Korea (no. 20016290), National Research Foundation of Korea (NRF) grant funded by the Korean government (MSIT) (no. 2021R1A2C2009521) and the Nano & Material Technology Development Program through the National Research Foundation of Korea (NRF) funded by Ministry of Science and ICT (RS-2023-00281346). All funding received by Y.R.D.

Author contributions

Y.R.D., H.M.C. and J.K.K. conceived and designed the research and Y.R.D. supervised the project. S.A., H.J.K. and Y.J.L. fabricated fin-ELDs and J.K.S. analyzed optical properties. M.K. and G.Y.Y. characterized structural properties using SEM and TEM. S.Y. and Y.K. fabricated assembled electrodes and performed the assembly process. S.L., E.H. and H.K. fabricated fin-LED based-EL Devices. S.L. interpreted EL data and characterized device properties. K.N.L. performed data analysis and image processing. Y.J.E. simulated the DEP assembly and analyzed simulation data. S.L., Y.J.E., and Y.R.D. wrote the manuscript, and all the authors reviewed it.

Competing interests

The authors declare no competing interests.

Additional information

Supplementary information The online version contains supplementary material available at https://doi.org/10.1038/s41467-024-53965-0.

Correspondence and requests for materials should be addressed to Young Rag Do.

Peer review information *Nature Communications* thanks the anonymous reviewer(s) for their contribution to the peer review of this work. A peer review file is available.